The Journal of Chemical Physics

RESEARCH ARTICLE | SEPTEMBER 26 2024

Optical force and torque in near-field excitation of C_3H_6: A first-principles study using RT-TDDFT

Risa Amano ; Daisuke Nishizawa ; Tetsuya Taketsugu ; Takeshi Iwasa

J. Chem. Phys. 161, 124110 (2024)
https://doi.org/10.1063/5.0223371
CHORUS

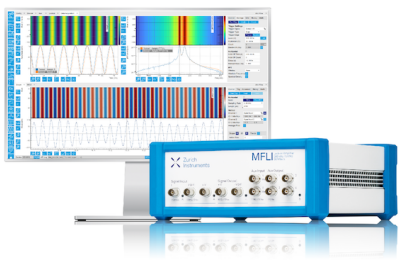

The Journal of Chemical Physics ARTICLE pubs.aip.org/aip/jcp

Optical force and torque in near-field excitation of C_3H_6: A first-principles study using RT-TDDFT

Cite as: J. Chem. Phys. 161, 124110 (2024); doi: 10.1063/5.0223371
Submitted: 13 June 2024 • Accepted: 3 September 2024 •
Published Online: 26 September 2024

Risa Amano,[1] Daisuke Nishizawa,[2] Tetsuya Taketsugu,[3,4] and Takeshi Iwasa[3,4,5,a)]

AFFILIATIONS

[1] Department of Physics, Graduate School of Science, Kyoto University, Kyoto 606-8502, Japan
[2] Graduate School of Chemical Sciences and Engineering, Hokkaido University, Sapporo 060-0810, Japan
[3] Department of Chemistry, Faculty of Science, Hokkaido University, Sapporo 060-0810, Japan
[4] WPI-ICReDD, Hokkaido University, Sapporo 001-0021, Japan
[5] PRESTO, Japan Science and Technology Agency, Kawaguchi 332-0012, Japan

[a)] **Author to whom correspondence should be addressed:** tiwasa@sci.hokudai.ac.jp

ABSTRACT

Optical trapping is an effective tool for manipulating micrometer-sized particles, although its application to nanometer-sized particles remains difficult. The field of optical trapping has advanced significantly, incorporating more advanced techniques such as plasmonic structures. However, single-molecule trapping remains a challenge. To achieve a deeper understanding of optical forces acting on molecular systems, a first-principles approach to analyze the optical force on molecules interacting with a plasmonic field is crucial. In our study, the optical force and torque induced by the near-field excitation of C_3H_6 were investigated using real-time time-dependent density functional theory calculations on real-space grids. The near field from the scanning tunneling probe was adopted as the excitation source for the molecule. The optical force was calculated using the polarization charges induced in the molecule based on Lorentz force. While the optical force and torque calculated as functions of the light energy were in moderate agreement with the oscillator strengths obtained from the far-field excitation of C_3H_6, a closer correspondence was achieved with the power spectrum of the induced dipole moment using near-field excitation. Time-domain analysis of the optical force suggests that the simultaneous excitation of multiple excited states generally weakens the force because of mismatches between the directions of the induced polarization and the electric field. This study revealed a subtle damping mechanism for the optical force arising from intrinsic electronic states and the influence of beating.

I. INTRODUCTION

The many controllable parameters of light, such as its amplitude, phase, and polarization, make it an attractive tool for manipulating the properties and reactivity of molecules. In addition to manipulating the molecular physicochemical properties, light can exert a force on molecules, thus enabling their position to be controlled. Following the experimental observation of radiation pressure[1] and the establishment of methods for generating strong laser fields, Ashkin reported the first optical trapping of micrometer-sized dielectric spheres by tightly focusing a laser beam with a lens.[2] Later, Ashkin *et al.*, demonstrated that a single laser beam could be used to trap and manipulate microparticles. This finding paved the way for the application of optical forces[3] and led to the development of a technique known as "optical tweezers." Researchers have shown that this technique could be used to trap and manipulate red blood cells,[4] stem cells,[5] DNA,[6,7] and biomolecular motors[8,9] modified with dielectric spheres; consequently, it has made significant contributions to the fields of cell and molecular biomechanics and has since become a widely used tool in these areas.

However, although laser trapping has proved to be an effective tool for manipulating micrometer-sized particles, its application to nanometer-sized particles remains challenging. This is because the trapping force, that is, the gradient force, cannot overcome the Brownian motion as the laser light cannot be focused onto a region smaller than half of its wavelength owing to the diffraction limit. This challenge has been overcome by developing plasmonic nanotweezers.[10–16] The use of plasmonic structures, such as gold bowties or gold nanoparticles, makes it possible to confine electric fields to deep subwavelength regions because of the localized surface plasmon resonance (LSPR).[17] The gradient force produced by a plasmonic nanotweezer can thus surpass that achieved with

conventional optical tweezers because the gradient force is proportional to the gradient of the field intensity. LSPR enables the manupilation of nanometer-sized plasmonic materials,[18,19] single proteins[20] and DNA,[21] and macromolecular assemblies.[22] In addition, a nanostructured semiconductor-assisted (NASSCA) optical tweezer, which exploits the enhancement of an electric field by the nanospikes on metal-free black silicon, was developed[23] and subsequently used to control polymer chains.[24]

The possibility of single-molecule trapping was theoretically demonstrated shortly after the advent of plasmonic nanotweezers;[25] however, the experimental realization thereof has remained difficult. Unlike spherical nanoparticles, molecules have unique shapes and orientations, and their electronic states must additionally be considered. Therefore, molecular polarizability varies, depending on the choice of molecules and the molecular orientation in the optical field. Because the gradient force is proportional to the polarizability of a material, the polarizability of molecules is crucial for molecular manipulation. The remaining targets for controlling materials with the use of light are, therefore, molecules, and single-molecule control is currently attracting researchers' keen attention.[26,27] In recent years, several studies describing the use of plasmonic nanotweezers to trap molecular assemblies have been reported,[28–30] and small molecules have also been successfully controlled at room temperature.[31,32] Attempts have been made to enhance the optical force by controlling the excitation state using chemical modifications.[33] An additional advancement involved the development of photoinduced force microscopy, which uses optical force detection with a scanning probe microscope to map the morphology and chemical properties.[34,35] This technique was subsequently used to visualize the optical response of single molecules.[36] These results suggest the importance of target molecule selection, which points to the future need for a method that would allow the optical force of any molecule to be analyzed.

In our previous study, we developed an optical-force analysis method based on time-dependent density functional theory (TDDFT) for simple spherical systems.[37] In this study, we extend our method to nonspherical molecules and develop a method with which to analyze the optical torque, in addition to the optical force. Our first-principles-based approach directly incorporates the electronic states of molecules into the force analysis and enables a detailed analysis of the forces experienced by any molecule and its light characteristics. Time-domain analysis is performed to clarify the relationship among the excited states of molecule, induced polarization, and optical force and torque. For future reference, we will discuss an outlook of the optical forces in near-field excitation from the perspective of the wave function. Our method is expected to significantly contribute to progress in the manipulation of molecules with the use of light.

II. THEORY

In this study, we employed a real-time real-space (RT-RS) differential method to solve the time-dependent Kohn–Sham (TD-KS) equation. The TD-KS equation is expressed as follows for the wavefunction of the jth orbital $\psi_j(\mathbf{r},t)$:

$$i\hbar\frac{\partial}{\partial t}\psi_j(\mathbf{r},t)=\left[-\frac{\hbar^2}{2m}\nabla^2+V_{\mathrm{KS}}[\rho_e](\mathbf{r},t)\right]\psi_j(\mathbf{r},t), \tag{1}$$

where m represents the electron mass and ρ_e represents the electron density for closed-shell systems,

$$\rho_e(\mathbf{r},t)=2\sum_{j=1}^{N/2}|\psi_j(\mathbf{r},t)|^2. \tag{2}$$

The KS potential $V_{\mathrm{KS}}[\rho_e](\mathbf{r},t)$ is a function of ρ_e and comprises the electron–ion interaction potential $V_{\mathrm{ion}}(\mathbf{r})$, time-dependent Hartree potential, the exchange–correlation potential $V_{\mathrm{xc}}[\rho_e](\mathbf{r},t)$, and external field potential $V_{\mathrm{ext}}(\mathbf{r},t)$,

$$V_{\mathrm{KS}}[\rho_e](\mathbf{r},t)=V_{\mathrm{ion}}(\mathbf{r})+\frac{1}{4\pi\varepsilon_0}\int d\mathbf{r}'\frac{\rho_e(\mathbf{r}',t)}{|\mathbf{r}-\mathbf{r}'|}+V_{\mathrm{xc}}[\rho_e](\mathbf{r},t)+V_{\mathrm{ext}}(\mathbf{r},t). \tag{3}$$

A norm-conserving pseudopotential was employed for the electron–ion interaction potential of each atom.

Using the obtained electron density, optical force was calculated using the Lorentz force between the induced polarization charges and near field,

$$\mathbf{F}(t)=\int d\mathbf{r}\mathbf{F}(\mathbf{r},t), \tag{4}$$

$$\mathbf{F}(\mathbf{r},t)=-[\rho_e(\mathbf{r},t)-\rho_e(\mathbf{r},0)]\mathbf{E}(\mathbf{r},t). \tag{5}$$

The torque was obtained as follows:

$$\mathbf{N}(t)=\int d\mathbf{r}[\mathbf{r}\times\mathbf{F}(\mathbf{r},t)]. \tag{6}$$

Finally, the time average of these values gives the effective optical force and torque for a pulsed near field of duration T,

$$\langle\mathbf{F}\rangle=\frac{1}{T}\int_0^T dt\mathbf{F}(t), \tag{7}$$

$$\langle\mathbf{N}\rangle=\frac{1}{T}\int_0^T dt\mathbf{N}(t). \tag{8}$$

III. MODEL AND COMPUTATIONAL DETAIL

We study cyclopropane (C_3H_6) excited by near field. The near field is modeled by generating in the vicinity of a scanning tunneling microscopy (STM) tip. The model system and near-field distributions are shown in Fig. 1. The near field around the tip was modeled using a point dipole field expressed by the following equation:

$$\mathbf{E}^{\mathrm{nf}}(\mathbf{r})=\frac{[3\mathbf{n}(\mathbf{n}\cdot\mathbf{p})-\mathbf{p}]}{4\pi\varepsilon_0\mathbf{r}^3}, \tag{9}$$

where $\mathbf{n}$ is the normalized coordinate vector and $\mathbf{p}$ is the dipole moment. The near field under the tip has radial distributions.[38] The interaction Hamiltonian between the near field and the molecule in the minimal coupling form is given by the corresponding scalar potential,[39]

$$\phi(\mathbf{r};\mathbf{R})=\frac{(\mathbf{r}-\mathbf{R})\cdot\mathbf{p}}{4\pi\varepsilon_0|\mathbf{r}-\mathbf{R}|^3}. \tag{10}$$

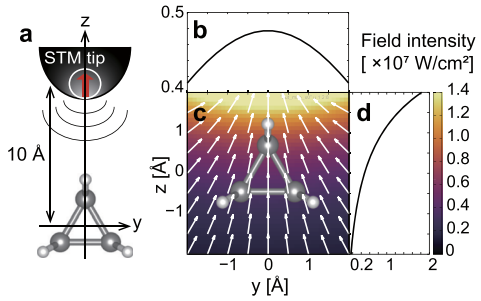

FIG. 1. (a) Computational model of C_3H_6 under the STM tip. The red arrows represent the light source dipole, (b) electric field intensity along the *y* axis, (c) electric field lines (white arrows) and electric field intensity map on the *yz* plane, and (d) the electric field intensity along the *z* axis.

Compared to the near field around the tip, which was simulated using the finite element method, the electric field distribution is qualitatively consistent.[40] While quantitative differences in intensities, particularly in the lateral vs vertical intensity ratio, can occur, we expect similar results even when using a coupled Maxwell-TDDFT approach to obtain the near field between the tip and surface. The near field beneath the tip would still exhibit a radial distribution on the surface. Direct inclusion of the tip into the first-principles calculations by using a single atom or a cluster model is also a promising improvement.[41]

The distance between the molecular center and the point dipole of 0.1 Debye is 10 Å. An STM tip-enhanced Raman spectroscopy (STM-TERS) study showed that the intrinsic vibrational modes of the target molecule were unaffected when the distance between the tip and the molecule was 5.8 Å.[42] Therefore, chemical interactions such as charge transfer and other perturbations can be very weak or even ruled out in the present model. The electric field lines and intensities are shown in Figs. 1(b)–1(d). The electric field mainly existed along the *z* axis of the molecule, and the intensity of the field has a steep gradient along this axis.

The geometry of C_3H_6 was optimized using TURBOMOLE[43–45] at the Perdew–Burke–Ernzerhof (PBE)[46,47]/aug-cc-pVDZ[48,49] level, followed by the excited states calculation for basic understanding of the molecule. All the remaining DFT and TDDFT calculations were performed using the real-time and real-space TDDFT program SALMON.[50] The PBE density functional and a norm-conserving Troullier–Martins type of pseudopotential[51] that were generated with fhi98PP software[52] were used. The calculation space was a cube with a side length of 20 Å centered on the molecule and a mesh width of 0.25 Å. Real-time propagation was performed for up to 20 fs with a time step of 0.001 25 fs.

The absorption spectrum was obtained using a δ pulse method,[53] where the ground state wavefunction perturbed by $e^{(i\delta\boldsymbol{k}\cdot\boldsymbol{r})}$ ($|\delta\boldsymbol{k}|$ = 0.01 a.u.) was used as the initial wavefunction for real-time propagation with the molecular Hamiltonian (i.e., without any external fields).

For real-time propagation in the near field, the external potential is expressed by the following equation:

$$V_{\mathrm{ext}}(\mathbf{r};\mathbf{R},t;\omega) = \phi(\mathbf{r};\mathbf{R})f(t;\omega). \tag{11}$$

We assumed that the electric field oscillates at a frequency of ω. The time profile $f(t)$ of the electric field is given by

$$f(t;\omega) = \sin(\omega t)\cos^2\left(\frac{\pi}{2}\cdot\frac{t-3t_0}{t_0}\right). \tag{12}$$

A pulse duration of 20 fs (t_0 = 10 fs) was used for the calculations.

The time average of the optical force and torque was determined by using a time step of 0.031 25 fs to limit the storage requirements by reducing the number of required files; for the integration, electron densities were stored as a cube file. The integration using Eq. (4) was, therefore, carried out every 25 steps of the real-time propagation.

A short-time Fourier transform (STFT) was used to analyze the dynamics,

$$f(t,\omega) = \int_{t-\frac{T}{2}}^{t+\frac{T}{2}} w(t'-t)f(t')e^{-i\omega t'}\,dt', \tag{13}$$

where T is the width of the window function and the energy resolution was set to 0.01 eV. The window function is expressed as

$$w(t) = 1 - 3(t/T)^2 + 2(t/T)^3. \tag{14}$$

The STFT was performed by repeatedly shifting the center at constant intervals of Δt. The parameters for the induced dipole moment were set as follows: T = 1 fs, Δt = 0.1 fs, and $1 \le t \le 19$ fs. The parameters for the optical force were set as follows: T = 3.125 fs, Δt = 0.031 25 fs, and $3.125 \le t \le 16.906\,25$ fs.

IV. RESULTS AND DISCUSSION

A. Static properties

Figure 2 shows the structural and electronic properties of C_3H_6 obtained by TURBOMOLE. After geometry optimization, the C–C and C–H bond lengths are 1.52 and 1.10 Å, respectively. The frontier orbitals and their corresponding energies are shown in Fig. 2(b). The electronic transitions up to the seventh singlet excited state are also indicated there. HOMO and LUMO are *d* orbital-like, while LUMO+1 and LUMO+2 are *p* orbital-like. The absorption spectrum shown in Fig. 2(c) indicates that S_1–S_6 are very weak or even forbidden, as the *d*–*d* and *d* (in-plane) to *p* (out-of-plane) transitions are forbidden in an atom. S_5 to S_8 are in-plane *d*–*p*-like transitions. While all these excited states consist of doubly degenerate HOMOs and LUMO+2s transitions, S_7 and S_8 have strong oscillator strengths, but S_5 and S_6 are forbidden. This is in accordance with Nakai's pseudo-degenerate transition rule, which states that "*(i) The highest transition among transitions between degenerate orbitals is dipole-allowed; (ii) The excitation energy of the highest transition is larger than those of the other transitions.*"[54,55]

In this study, we focus on the lowest-lying excited states, including at least one strong optically allowed excited state. Within the energy range studied, we observe a strong peak attributed to S_7 and S_8 and a small peak attributed to S_1 and S_2. Although the exact excited state energies from TURBOMOLE and SALMON do not match precisely, the spectral shapes exhibit good agreement. Therefore, we believe that a qualitative picture of the excited states is shared by both methods/software. Moreover, by shifting the energy

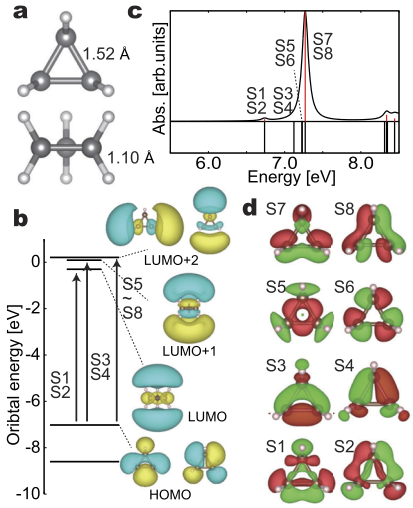

FIG. 2. Structural and electronic properties of C_3H_6 obtained by TURBOMOLE. (a) Top and side views of the optimized structure and its interatomic distances. (b) The frontier orbitals and their corresponding energies. (c) The absorption spectrum. The black lines indicate the position of electronic excitations. (d) The transition densities for these excited states.

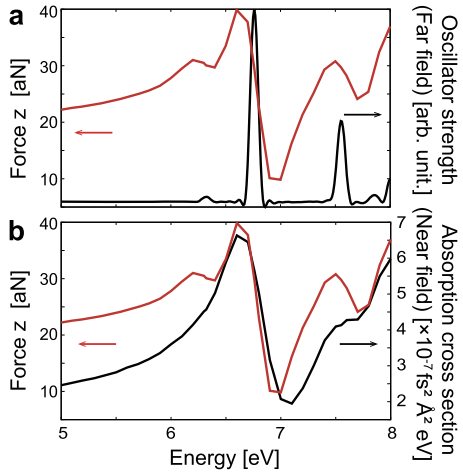

FIG. 3. Time-averaged optical force in the z-direction (red curve) and (a) oscillator strength for z-polarized far-field light (black curve) and (b) absorption cross section for near-field light (black curve) as a function of the incident energy.

scale by ~0.5 eV, the two absorption spectra align well. This energy discrepancy likely arises from the Rydberg nature of cyclopropane's unoccupied orbitals, as shown in Fig. 2(b). In TURBOMOLE, we employ the aug-cc-pVTZ basis set, which is among the largest available atomic orbital basis sets. In SALMON, we utilize a real-space box of substantial size that can stabilize these Rydberg states, resulting in lower excited state energies.

Figure 2(d) shows the transition densities[56] for these excited states. As we discussed previously, the transition density corresponds to the electron density differences obtained in the RT-TDDFT.[57] While the transition densities shown in the left column (S_1, S_3, S_5, and S_7) show symmetric distribution with respect to the molecular axis, those in the right (S_2, S_4, S_6, S_8) show anti-symmetric distributions. As shown in Fig. 1(c), the near field is symmetric with respect to the molecular axis if the tip is on the molecular axis. Therefore, the excited states with anti-symmetric transition densities will not be excited.

B. Optical force

Figure 3(a) shows the z component of the optical force induced by the near field and the oscillator strength, that is, the absorption spectrum for the far field. It should be noted that the optical force is induced by the near field, whereas the oscillator strength is obtained from the dipole moment induced by far-field excitation. The incident energy of the near-field light was varied from 5 to 8 eV in increments of 0.1 eV. In addition, three specific resonance energies at 6.32, 6.76, and 7.55 eV were also investigated.

The optical force was induced in the positive z-direction, where the intensity of the near field was strong. This confirmed that the gradient force was induced by the intensity gradient. The optical force is not induced in the x and y directions because of the symmetry of the near field, in which the intensity gradient on the molecule is canceled out, as shown in Fig. 1(b).

The optical force and absorption spectra exhibit similar spectral shapes. The position of the peak in the absorption spectrum represents the inherent excitation energy of the molecule. Resonant excitation occurs when the incident energy corresponds with the inherent excitation energy. Figure 3(a) shows the tendency of the optical force to increase under the resonance conditions. This tendency has been demonstrated in both experimental[58] and theoretical[59–61] studies. The optical force is enhanced because the molecule is strongly polarized by the resonance. However, closer inspection reveals that discrepancies exist between the optical force and oscillator strength. The optical force reached a maximum at 6.60 eV, which was shifted to a slightly lower energy than the resonance condition, and the optical force weakened at the resonance condition of 6.76 eV. Furthermore, the optical force is significantly weakened and is minimized at 7.00 eV, which is between the two adjacent resonance conditions of 6.76 and 7.55 eV. These discrepancies were discovered by conducting a detailed analysis of the electronic states. As the optical force is expressed by Eq. (5), these decreases in the optical force observed near the resonance condition suggest the existence of a strong relationship between the polarization of the molecule and the external field.

Figure 3(b) shows the z-component of the optical force and absorption cross section, both of which are from the near field. The "absorption cross section" is obtained by integrating the Fourier transform of the dipole moment induced by the near-field light in the energy range from 0 to 10 eV. In this energy range, only one peak was observed, irrespective of the frequency of the applied near field. The integration was performed with an energy step of 0.1 eV. The absorption cross section represents the amount of light energy absorbed to induce a dipole moment on the molecule. Overall, the spectral shapes of $\langle F_z \rangle$ and the absorption cross section for near-field light are in very good correspondence. While the optical force exhibits a small peak at 6.2 eV and the oscillator strength also

displays a small peak at 6.3 eV, the absorption cross section lacks a corresponding peak. This discrepancy in the near-field cross section might be attributed to the low energy resolution of the spectrum. While optical force spectra are derived from the time average, the near-field absorption cross section is computed by integrating the induced dipole moment over a specific energy range. This integration process can broaden the main peak, causing it to overlap with the small peak. As the absorption cross section was well correlated with the optical force, we analyzed the time profile of the induced dipole moments and optical forces in detail. In the following, the optical force in the z-direction under off-resonance (5.00 eV), on-resonance (6.76 eV), and minimum (7.00 eV) conditions are analyzed in depth.

Figures 4(a) and 4(b) show the time profiles of the z-components of the optical force F_z and the induced dipole moment d_z, respectively, whereas Fig. 4(c) shows the Fourier transform of the induced dipole moment under the off-resonance condition. The insets show snapshots of the difference in electron density $[\rho_e(\mathbf{r},t) - \rho_e(\mathbf{r},0)]$ when the optical force reaches its maximum and minimum values, where red and blue represent the positive and negative charges, respectively. In Fig. 4(b), the induced dipole moment is shown in red, whereas the black line shows the time profile of the external field. The amplitude of the external field was adjusted to make it easier to observe the difference in phase between the polarization and external field. Figure 4(d) shows the relationship between the electric field, induced charges, and optical force. Figures 4(e) and 4(f) show the maps $d_z(x_0,y,z)$ and $F_z(x_0,y,z)$ at 10.63 fs when the optical force reaches a maximum, respectively, in a plane closest to the molecular plane (x_0 = 0.24 Å, see axes for Fig. 1).

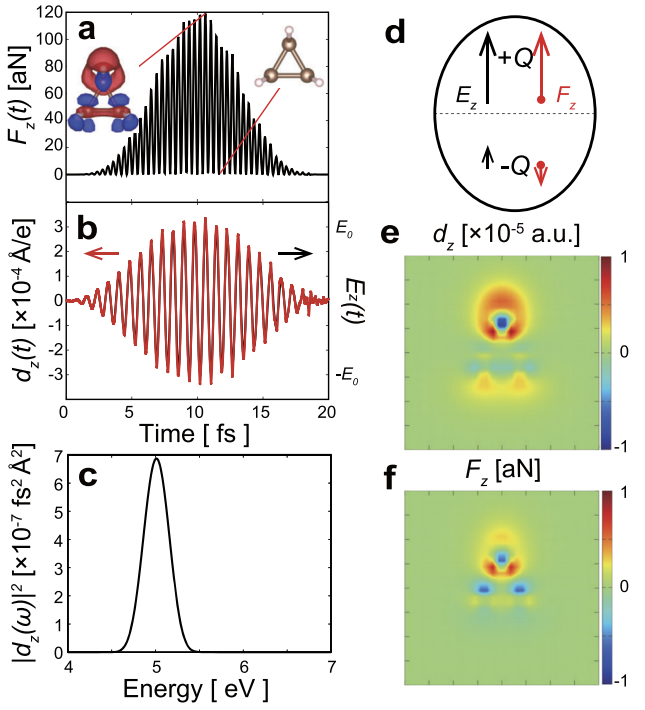

FIG. 4. (a) Optical force with snapshots of the differences in the electron density, (b) induced dipole moment (red) and applied pulse (black) in time-domain, and (c) the power spectrum of the induced dipole moment under the off-resonance condition at 5.00 eV. (d) The schematic for the mechanisms of the optical force. Maps of (e) d_z and (f) F_z in a plane closest to the molecular plane (i.e., 0.24 Å above the molecular plane) at 10.63 fs when the optical force reaches a maximum under the off-resonance condition. For the electron density difference in the inset of panel (a), the red and blue colors show positive and negative charges.

Under off-resonance conditions, the optical force is always positive, as shown in Fig. 4(a), and directs the molecule toward the tip. In addition, as shown in Fig. 4(b), the phases of the polarization and the near field are always aligned. The relative phase between the polarization and the electric field is crucial because it determines the direction of the optical force. As shown in Fig. 4(d), $E_z > 0$ causes $d_z > 0$, in which the molecule is simplified as a dipole with positive and negative induced charges in its upper and lower parts, respectively. The near field is stronger for the upper part due to the intensity gradient, resulting in a larger F_z in the upper part compared to the lower part. Consequently, a positive net optical force toward the tip arises under off-resonance conditions. The dipole and optical force fields exhibit a strong correlation, as shown in Figs. 4(e) and 4(f).

Under on-resonance conditions, a negative force was observed in the later part of the near-field excitation, as shown in Fig. 5(a). The induced dipole moment increased constantly and did not decrease even after the near field was turned off, as shown in Fig. 5(b). The strong polarization continued to prevail even when the external field weakened. This is a characteristic of forced oscillation.[62,63] When on resonance, the amplitude of the induced oscillation increases linearly with time. This behavior is also observed using real-time TDDFT and discussed.[64] Under resonance conditions, the inherent characteristics of the electronic excited states in resonance become more pronounced, whose spatial distributions do not necessarily align with those of the applied near field. When the optical force reaches its maximum at 11.09 fs, d_z and F_z exhibit patterns similar to those observed under the off-resonance condition, as shown in Figs. 5(f) and 5(g), while the intensity distribution no longer simply follows that of the near-field pattern. This is clearer when the optical force reaches its minimum at 13.72 fs. Comparing Fig. 5(d) with those of Fig. 2(d), the electron density difference for min at 13.72 fs can be attributed to the S_7 excited state. The charge distribution for the maximum and minimum time is simplified to Fig. 5(e), where the upper part is divided into positive and negative, while the lower part remains unchanged as the detail of the upper part is more important due to the stronger field intensity. As shown in Figs. 5(d) and 5(f), the charge distribution and the dipole field in the upper part is opposite for the maximum and minimum time, resulting in the larger positive and negative forces exerted on the upper part of the molecule, as shown in Figs. 5(e) and 5(g).

Finally, we discuss the force minimum condition at 7.0 eV shown in Fig. 3. When the optical force is minimized, the direction of the optical force is reversed from positive to negative, as shown in Fig. 6(a). This reversal occurred at 13 fs and coincided with a node in the beat pattern of the induced polarization, as shown in Fig. 6(b). Figure 6(c) shows magnified views of the regions 0–5 and 11–16 fs. In the former of these two time windows, the phases of the external field and the induced dipole moment corresponded. However, beyond the node at 13 fs, the external field and polarization became anti-parallel, resulting in a negative optical force, as

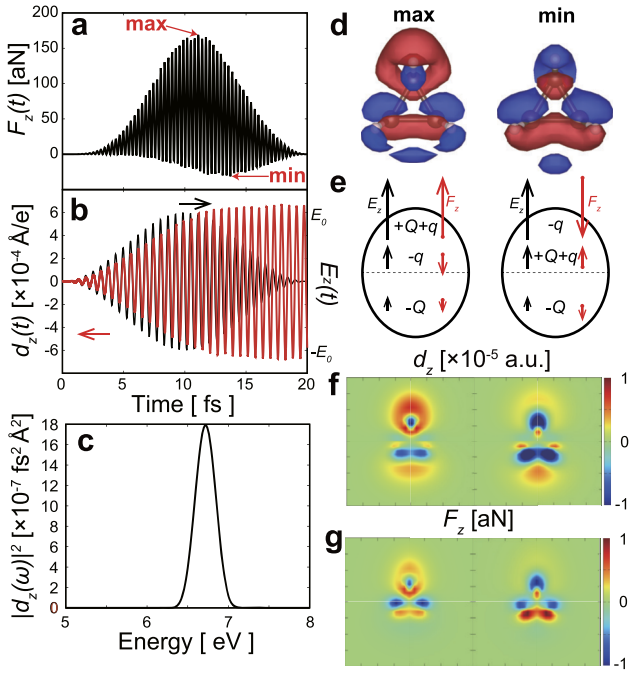

FIG. 5. Time profile of (a) optical force and (b) induced dipole moment (red) and applied pulse (black), and (c) the power spectrum of the induced dipole moment under an on-resonance condition at 6.76 eV. (d) Electron density difference where the red and blue colors show positive and negative charges, respectively, (e) the schematic for the mechanisms of the optical force, and maps of (f) d_z and (g) F_z in a plane closest to the molecular plane (i.e., 0.24 Å above the molecular plane) at 11.09 fs when the optical force reaches a maximum in the left and at 13.72 fs when the optical force reaches a minimum in the right.

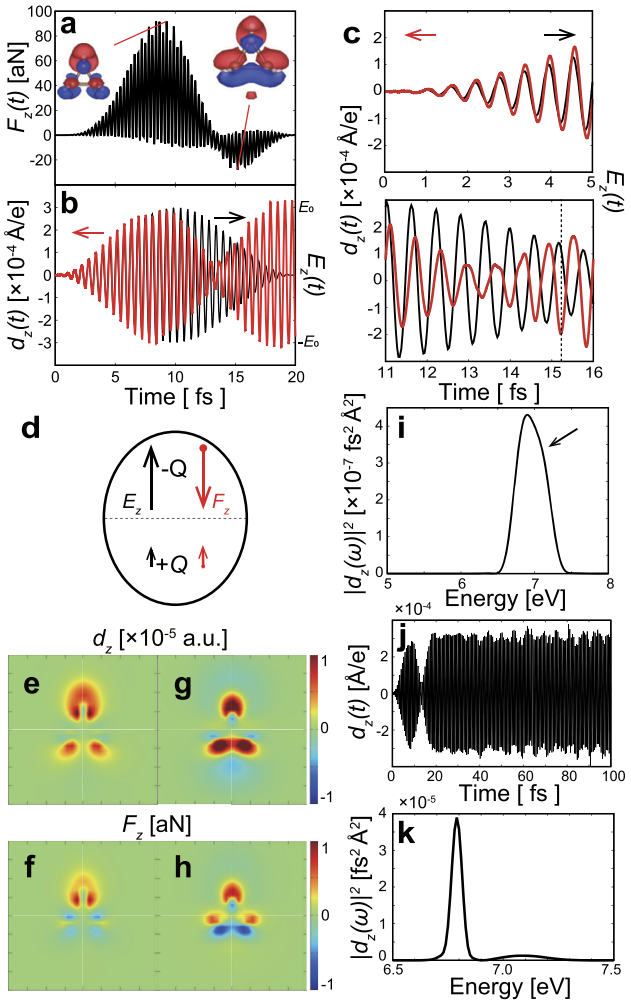

FIG. 6. (a) Optical force with snapshots of electron density differences at 9.28 fs and 15.19 fs and (b) and (c) induced dipole moment (red) and applied pulse (black) in the time domain. (d) Schematic for optical force. Maps of [(e) and (g)] d_z and [(f) and (h)] F_z at 9.28 and 15.19 fs, respectively, corresponding to the electron density differences shown in the inset of panel (a). (i) Power spectrum of d_z. (j) Time-profile of the induced dipole moment for longer time-propagation and (k) the corresponding power spectrum.

shown in Fig. 6(d). This negative force contributed to the minimum observed time-averaged optical force. When the optical force reaches its maximum at 9.28 fs, the electron density difference and the maps of d_z and F_z resemble those shown in Figs. 4 and 5. In contrast, when the optical force reaches its minimum at 15.19 fs, where the induced dipole moment and electric field is anti-parallel, these appear different, as shown in Figs. 6(a), 6(g), and 6(h). In the latter part of the dynamics, the induced polarization charge distribution opposed that of the electric field due to the beat, thereby extending the negative net optical force for longer duration compared to other conditions. Consequently, the time average of the optical force decreases.

Let us analyze the beat. As shown in Fig. 6(i), the power spectrum consists of a broad peak with a shoulder, indicated by the arrow. The peak position is shifted from the incident energy of 7.00 to 6.90 eV, with the appearance of the shoulder at 7.12 eV. The superposition of these two waves results in a beat. The shift in the peak position was attributed to the resonance state at 6.76 eV. To confirm this hypothesis, a longer TDDFT calculation was performed for up to 100 fs using the same pulse duration of 20 fs. The resulting time profile and Fourier transform are shown in Figs. 6(j) and 6(k), respectively. The Fourier transform now exhibits a sharp peak at 6.79 eV, very close to the resonance energy of 6.76 eV, along with a smaller peak at 7.1 eV, which is also considered to originate from the resonant state at 7.55 eV. Even after the pulse was discontinued, the induced dipole moment continued to oscillate at a frequency corresponding to the resonant state (6.76 eV). This behavior occurs because a short pulse encompasses a broader range of frequencies than the applied field frequency (7.0 eV), thereby exciting the resonance state closest to the energy.

We have summarized the electron dynamics induced by the near field. Under off-resonance conditions, the electrons are forced to oscillate by the electric field, and the induced dipole moment vanishes upon the electric field's termination. To interpret, light absorption does not occur. Under resonant conditions, the induced dipole moment persists after the pulse ends, a behavior attributable to light absorption by the molecule. Under minimum conditions, multiple excited states are excited, leading to beating in electron

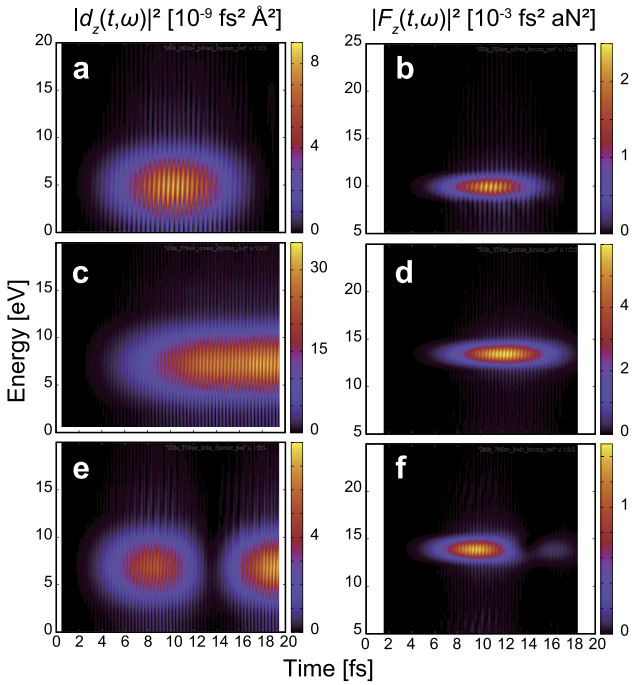

FIG. 7. Short-time Fourier transform plot for [(a), (c), and (e)] the induced dipole moment and [(b), (d), and (f)] optical force as a function of energy and time under [(a) and (b)] off-resonance (5.00 eV), [(c) and (d)] on-resonance (6.76 eV), and [(e) and (f)] optical force minimum conditions (7.00 eV).

oscillations. Consequently, the duration of the envelope function for the induced dipole moment differs from that of the applied field. The resonance effects and multiple excitations can cause negative force in the time profile, decreasing the net optical force. While the energy spectrum of optical force generally resembles that of induced polarization, there are deviations owing to multiple reasons arising from the quantum mechanical nature of the molecular electronic structure.

To visualize the energy dependence of the induced dipole moment and optical force, STFT analysis were applied to both quantities using Eq. (13) and plotted against time, as shown in Fig. 7. The frequency of the optical force is twice the frequency of the induced dipole moment because the force is proportional to the product of the induced polarization and electric field, both of which exhibit harmonic time dependence. This energy dependence numerically confirmed the adequacy of the present calculations. Although the induced dipole moment and optical force are not directly correlated, they exhibit similar behavior. The optical force exhibits a narrower energy distribution than the induced dipole moment, as the force also depends on the electric field.

The dependence of the optical force on the intensity of the near field was also investigated. The relationship between the time-averaged near-field intensity at the center of mass of the molecule and optical force is shown in Fig. 8. By varying the source dipole moment from 0.001 D to 100 D, the near-field intensity at the center of mass of the molecule was varied from 10^3 to 10^{13} W/cm^2. The period and duration of the pulsed electric field were fixed at 20 fs,

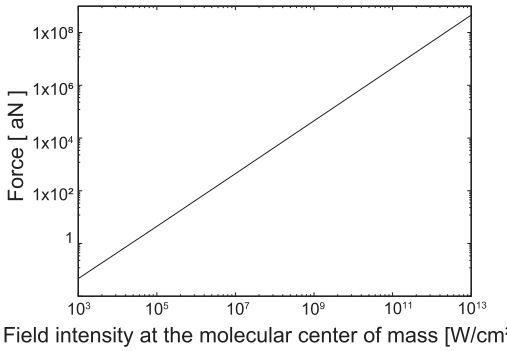

FIG. 8. Log–log plot of time-averaged near-field intensity at the center of mass of the molecule and optical force in the *z* direction.

and the incident energy was fixed at 5 eV (off-resonance condition). In the near-field intensity range from 10^3 to 10^{13} W/cm^2, the magnitude of the optical force was proportional to this intensity. For light of which the intensity exceeded 10^{13} W/cm^2, the calculation became impossible because of ionization. Even in the presence of an intense light field, the optical force depended linearly on the field strength. However, in such an intense light field, if applied, fragmentation might occur, particularly when (multiple) ionization takes place. Even higher field intensities can cause multiple ionizations, ultimately resulting in Coulomb explosion.[65]

As shown in Fig. 9(a), at an intensity of 10^7 W/cm^2, the first-order peak intensity is 10^6 times larger than the second-order or higher peaks. The contribution of the linear response was large, whereas the influence of the nonlinear response was considered negligible. However, at 10^{11} W/cm^2, higher-order responses were clearly observed, indicating the stronger influence of the nonlinear response than at 10^7 W/cm^2. Nevertheless, the linear relationship shown in Fig. 8 suggests that the nonlinear response never exceeds the linear response. The time-averaged optical force in the *z* direction and the oscillator strength of the *z*-polarized light for near-field intensities of 10^7 and 10^{11} W/cm^2 at the center of mass of the molecule are shown in Fig. 9(b). The qualitative relationship between the incident energy and optical force is generally unchanged by the linear and nonlinear responses. Quantitatively, upon exposure to high-intensity light, the peak of the optical force near the resonance condition of 7.55 eV undergoes slight redshift. The deviation may come from the fact that the polarization becomes more complex due to the nonlinear response.

C. Optical torque

The amount of torque that is generated by breaking the symmetry of the molecule near the field was investigated by analyzing the optical force and torque by changing the relative orientation of the molecule near the field. Schematic diagrams of the three different excitation models are shown in Figs. 10(a)–10(c); the time-averaged optical force for each of these models is shown in Figs. 10(d)–10(f); and the time-averaged torque is shown in Figs. 10(g)–10(i).

Because the point group of C_3H_6 is D_{3h}, Model a, in which the light source is aligned with the C_2 symmetry axis, represents the

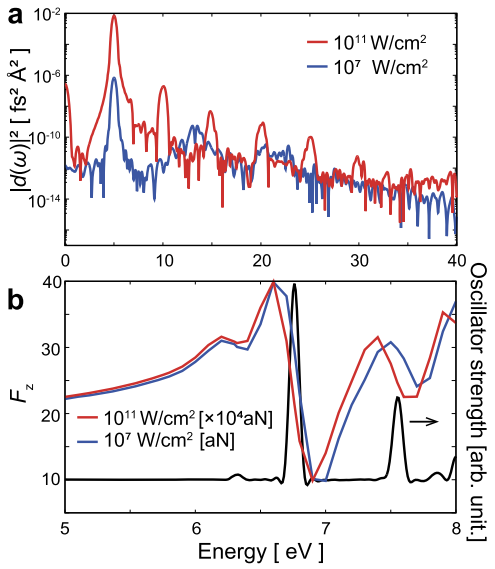

FIG. 9. (a) Power spectra of the induced dipole moment for an incident energy of 5 eV. The red curve corresponds to a near-field intensity of 10^{11} W/cm^2 at the molecular center, whereas the blue curve corresponds to an intensity of 10^7 W/cm^2. (b) Time-averaged optical force (red and blue) and oscillator strength (black). Again, the red and blue curves correspond to a near-field intensity of 10^7 and 10^{11} W/cm^2, respectively.

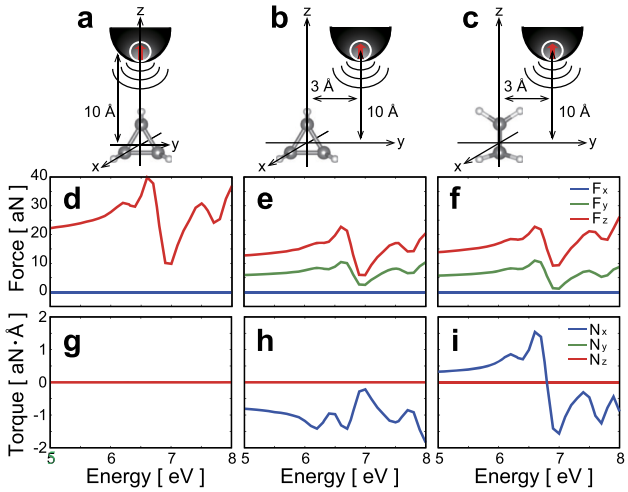

FIG. 10. (a)–(c) Excitation model, (d)–(f) time-averaged optical force, and (g)–(i) optical torque. The blue, green, and red lines represent x, y, and z component of force and torque, respectively. The torque is defined as positive for counterclockwise rotation around the axis.

orientation with the highest symmetry of the combined system consisting of the molecule and the near field. In Model b, the light source was shifted by 3 Å in the y direction relative to Model a, and in Model c, the molecule in Model b was rotated around the z axis by 90°. As shown in Fig. 10(g), no torque was generated in Model a. However,

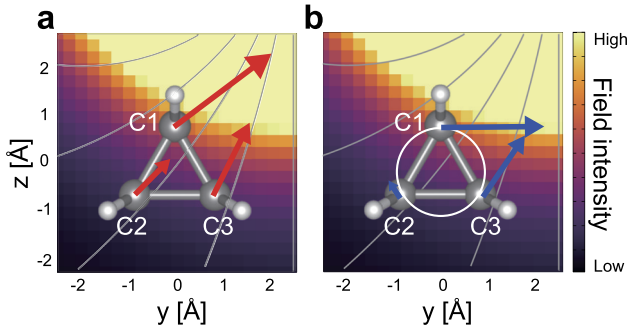

FIG. 11. Mechanism of optical torque generation in Model b. (a) Induced optical forces on each carbon atom (red arrows). (b) Components perpendicular to the position vectors of the optical forces (blue arrows) and rotation trajectory of carbon atoms around the center of mass of the molecule (white circle). The background color map represents the electric field intensity, and the gray curves represent the electric field lines.

in Models b and c, in which the light source was not on the symmetry axis, an optical force was induced in the y and z directions, as shown in Figs. 10(e) and 10(f). The general shapes of the spectra were similar for both models. However, as shown in Figs. 10(h) and 10(i), the torque spectrum differs depending on the orientation. In both cases, the rotation axis is the x axis, but in Model (b), the rotation direction is clockwise and constant, whereas in Model (c), the torque changes from counterclockwise to clockwise at a resonance energy of 6.76 eV. This difference in the direction of rotation is attributable to the difference in the intensity distribution of the optical force caused by the orientation of the molecule. These results demonstrate the potential for controlling the molecular rotation by manipulating the molecular orientation and incident energy.

The amount of torque is determined by the relative orientation of the molecule with respect to the electric field. To investigate this mechanism, we used Model b and extracted the optical forces induced around the carbon atoms (C1, C2, and C3 shown in Fig. 11) for simplification. Figure 11(a) shows the sum of the optical forces induced around the carbon atom, indicated by the red arrows. The length of each arrow corresponds to the magnitude of the optical force. The color map represents the intensity of the electric field, and the gray lines represent the electric field. The direction and relative magnitude of the optical force can be determined by the fact that the optical force is induced in the direction of increasing electric field intensity and that the intensity gradient is larger in the region where the electric field lines are dense. The magnitudes of the optical forces are C1, C3, and C2 in decreasing order. In Fig. 11(b), the components perpendicular to the position vectors of the optical forces are extracted and indicated by the blue arrows. Considering that the molecule rotates around its center of mass, a force that drives clockwise rotation is induced in C1 and C2, and a force that drives counterclockwise rotation is induced in C3. Because the force driving the clockwise rotation is stronger, an optical force moment that rotates clockwise around the x axis is generated.

D. Future perspective

In this study, we investigated the optical forces and torques experienced by a molecule with fixed coordinates. The next step

would be to move the coordinates. As shown here, if we were to neglect the coupling between rotation and vibrations, the translational and rotational motions are driven only by the near field. Let us write the Hamiltonian H as

$$H = H_{\mathrm{mol}} + H_{\mathrm{int}}, \tag{15}$$

where H_{mol} and H_{int} represent the molecular Hamiltonian and the light-molecule interaction Hamiltonian, respectively. Because the molecular Hamiltonian neither depends on the position $\mathbf{g}$ nor the angle $\boldsymbol{\theta}$ of the molecule, we have

$$\frac{\partial H_{\mathrm{mol}}}{\partial \mathbf{g}} = \frac{\partial H_{\mathrm{mol}}}{\partial \boldsymbol{\theta}} = 0. \tag{16}$$

Conversely, the near field is spatially nonuniform; therefore, H_{int} depends on $\mathbf{g}$ and $\boldsymbol{\theta}$ as follows:

$$\frac{\partial E}{\partial \mathbf{g}} = \frac{\partial E_{\mathrm{int}}}{\partial \mathbf{g}} \neq 0, \tag{17}$$

$$\frac{\partial E}{\partial \boldsymbol{\theta}} = \frac{\partial E_{\mathrm{int}}}{\partial \boldsymbol{\theta}} \neq 0. \tag{18}$$

Actual computation may require a certain extent of approximation to reduce the computational cost. One promising approach would be to propagate a stroboscopic molecular motion in which the time-averaged forces are used for a short time, during which the atomic positions are approximately unchanged.[66]

To consider molecular vibrations, we would need to determine the forces acting on each atom. In this case, it would be more effective to use a molecular dynamics approach that includes all the translational, rotational, and vibrational motions. These forces originate from light and electrons whose spatial distributions are changed by light. The forces acting on the ith ion at $\mathbf{R}_i$ with charge Z_i are expressed as follows: the force from light,

$$\mathbf{F}^i_{\mathrm{int}} = \frac{Z_i}{T}\int dt \mathbf{E}(\mathbf{R}_i, t), \tag{19}$$

the force from electrons,

$$\mathbf{F}^i_{\mathrm{en}} = \frac{Z_i}{4\pi\varepsilon_0}\int d\mathbf{r}\frac{\mathbf{R}_i - \mathbf{r}}{|\mathbf{R}_i - \mathbf{r}|^3}\rho_e(\mathbf{r}), \tag{20}$$

and inter-ion repulsion,

$$\mathbf{F}^i_{\mathrm{nn}} = \sum_j \frac{1}{4\pi\varepsilon_0}\frac{Z_i Z_j}{|\mathbf{R}_i - \mathbf{R}_j|^3}(\mathbf{R}_i - \mathbf{R}_j). \tag{21}$$

These forces may be computed at certain time steps to average faster electron dynamics from the calculation. Alternatively, they can be computed by including the electron dynamics using TDDFT, such as the Ehrenfest approach[67,68] or the more cost-efficient Ehrenfest density functional tight-binding approach.[69,70]

A simple dipole field was adopted in this study as a near field; however, the use of multipolar formalism would allow the generalization of the near field to an arbitrary spatial distribution.[71] The multipolar Hamiltonian would enable the use of a near field that is obtained by solving Maxwell's equations.[72] Further improvements would require magnetic interactions to be considered for spin-polarized molecular manipulations.[73–77] In addition, a self-consistent treatment of light–matter interactions would be required to consider the interplay between molecules and light sources,[60,78,79] as well as a strong interaction between light and molecules for polaritonic hybridizations.[80] Solving the coupled Maxwell-TDDFT equations is a straightforward approach, yet computationally demanding.[81,82] Macroscopic quantum electrodynamics theory may solve these issues; however, the combination thereof with molecular dynamics remains a significant theoretical and computational challenge.[83–85]

V. CONCLUSIONS

We studied the optical force and torque induced by the near-field excitation of C_3H_6 under an STM tip using RT-TDDFT. In principle, the optical forces point toward the tip with a stronger field intensity. However, the resonance condition and simultaneous excitation of multiple excited states as a result of the short pulse can weaken the force. This can introduce a discrepancy between the far-field absorption spectrum and optical force and the torque spectra. The present study, performed from a quantum chemical perspective, deepens our understanding of the optical force in smaller materials, such as molecules, whose physicochemical properties depend strongly on their electronic structures. Although the present study only investigated the force and torque for a fixed molecular structure, in future studies, we aim to explicitly take into account the dynamics of the atoms to clarify and enable the active optical manipulation of the molecular properties, including the position, orientation, and excited states.

ACKNOWLEDGMENTS

T.I. acknowledges JST PRESTO, Japan (Grant No. JPMJPR20T1) and the Japan Society for the Promotion of Science (JSPS) KAKENHI (Grant Nos. 23K04671, 21H04644, 23K04833, and 23H03833) for financial support.

AUTHOR DECLARATIONS

Conflict of Interest

The authors have no conflicts to disclose.

Author Contributions

Risa Amano: Conceptualization (equal); Data curation (equal); Formal analysis (equal); Investigation (equal); Methodology (equal); Resources (equal); Software (equal); Validation (equal); Visualization (equal); Writing – original draft (equal); Writing – review & editing (equal). **Daisuke Nishizawa**: Visualization (supporting); Writing – review & editing (supporting). **Tetsuya Taketsugu**: Writing – review & editing (supporting). **Takeshi Iwasa**: Conceptualization (equal); Data curation (equal); Formal analysis (equal); Funding acquisition (equal); Investigation (equal); Methodology (equal); Project administration (equal); Resources (equal); Software (equal); Supervision (equal); Validation (equal); Visualization

(equal); Writing – original draft (equal); Writing – review & editing (equal).

DATA AVAILABILITY

The data that support the findings of this study are available from the corresponding author upon reasonable request.

REFERENCES

[1] E. F. Nichols and G. F. Hull, Phys. Rev. **13**, 307 (1901).
[2] A. Ashkin, Phys. Rev. Lett. **24**, 156 (1970).
[3] A. Ashkin, J. M. Dziedzic, J. E. Bjorkholm, and S. Chu, Opt. Lett. **11**, 288 (1986).
[4] R. Agrawal, T. Smart, J. Nobre-Cardoso, C. Richards, R. Bhatnagar, A. Tufail, D. Shima, P. H Jones, and C. Pavesio, Sci. Rep. **6**, 15873 (2016).
[5] H. De Belly, A. Stubb, A. Yanagida, C. Labouesse, P. H. Jones, E. K. Paluch, and K. J. Chalut, Cell Stem Cell **28**, 273 (2021).
[6] E. A. Abbondanzieri, W. J. Greenleaf, J. W. Shaevitz, R. Landick, and S. M. Block, Nature **438**, 460 (2005).
[7] J.-D. Wen, L. Lancaster, C. Hodges, A.-C. Zeri, S. H. Yoshimura, H. F. Noller, C. Bustamante, and I. Tinoco, Nature **452**, 598 (2008).
[8] A. Ashkin, K. Schütze, J. M. Dziedzic, U. Euteneuer, and M. Schliwa, "Force generation of organelle transport measured *in vivo* by an infrared laser trap," Nature **348**, 346–348 (1990).
[9] S. M. Block, L. S. B. Goldstein, and B. J. Schnapp, Nature **348**, 348 (1990).
[10] L. Novotny, R. X. Bian, and X. S. Xie, Phys. Rev. Lett. **79**, 645 (1997).
[11] K. Okamoto and S. Kawata, Phys. Rev. Lett. **83**, 4534 (1999).
[12] S. Kawata and T. Tani, Opt. Lett. **21**, 1768 (1996).
[13] V. Garcés-Chávez, R. Quidant, P. J. Reece, G. Badenes, L. Torner, and K. Dholakia, Phys. Rev. B **73**, 085417 (2006).
[14] Y. Zhang, C. Min, X. Dou, X. Wang, H. P. Urbach, M. G. Somekh, and X. Yuan, Light Sci. Appl. **10**, 59 (2021).
[15] K. B. Crozier, ACS Photonics **11**, 321 (2024).
[16] L. Novotny and B. Hecht, *Principles of Nano-Optics* (Cambridge University Press, 2012).
[17] R. Quidant, D. Petrov, and G. Badenes, Opt. Lett. **30**, 1009 (2005).
[18] S. Hong, O. Shim, H. Kwon, and Y. Choi, Anal. Chem. **88**, 7633 (2016).
[19] J. Rhie, D. Lee, T. Kim, S. Kim, M. Seo, D.-S. Kim, and Y.-M. Bahk, Nano Lett. **24**, 6753 (2024).
[20] Y. Pang and R. Gordon, Nano Lett. **12**, 402 (2012).
[21] T. Shoji, J. Saitoh, N. Kitamura, F. Nagasawa, K. Murakoshi, H. Yamauchi, S. Ito, H. Miyasaka, H. Ishihara, and Y. Tsuboi, J. Am. Chem. Soc. **135**, 6643 (2013).
[22] M. Toshimitsu, Y. Matsumura, T. Shoji, N. Kitamura, M. Takase, K. Murakoshi, H. Yamauchi, S. Ito, H. Miyasaka, A. Nobuhiro, Y. Mizumoto, H. Ishihara, and Y. Tsuboi, J. Phys. Chem. C **116**, 14610 (2012).
[23] T. Shoji, A. Mototsuji, A. Balčytis, D. Linklater, S. Juodkazis, and Y. Tsuboi, Sci. Rep. **7**, 12298 (2017).
[24] T. Nagai, K.-I. Yuyama, T. Shoji, Y. Matsumura, D. P. Linklater, E. P. Ivanova, S. Juodkazis, and Y. Tsuboi, ACS Appl. Nano Mater. **6**, 180 (2023).
[25] H. Xu and M. Käll, Phys. Rev. Lett. **89**, 246802 (2002).
[26] K. Setoura and S. Ito, J. Photochem. Photobiol., C **52**, 100536 (2022).
[27] H. Minamimoto, N. Oyamada, and K. Murakoshi, J. Photochem. Photobiol., C **55**, 100582 (2023).
[28] S. Ito, M. Mitsuishi, K. Setoura, M. Tamura, T. Iida, M. Morimoto, M. Irie, and H. Miyasaka, J. Phys. Chem. Lett. **9**, 2659 (2018).
[29] C. Pin, S. Ishida, G. Takahashi, K. Sudo, T. Fukaminato, and K. Sasaki, ACS Omega **3**, 4878 (2018).
[30] S. Ito, T. Mizoguchi, M. Mori, M. Koga, H. Sotome, M. Tamura, H. Ishihara, and H. Miyasaka, J. Phys. Chem. C **128**, 5206 (2024).
[31] N. Oyamada, H. Minamimoto, and K. Murakoshi, J. Am. Chem. Soc. **144**, 2755 (2022).
[32] Y. Kitahama, M. Funaoka, and Y. Ozaki, J. Phys. Chem. C **123**, 18001 (2019).
[33] R. Bresolí-Obach, S. Nonell, H. Masuhara, and J. Hofkens, Adv. Opt. Mater. **10**, 2200940 (2022).
[34] M. A. Almajhadi, S. M. A. Uddin, and H. K. Wickramasinghe, Nat. Commun. **11**, 5691 (2020).
[35] J. Yamanishi, H. Yamane, Y. Naitoh, Y. J. Li, N. Yokoshi, T. Kameyama, S. Koyama, T. Torimoto, H. Ishihara, and Y. Sugawara, Nat. Commun. **12**, 3865 (2021).
[36] T. Yamamoto, H. Yamane, N. Yokoshi, H. Oka, H. Ishihara, and Y. Sugawara, ACS Nano **18**, 1724 (2024).
[37] T. Iwasa and K. Nobusada, Phys. Rev. A **82**, 043411 (2010).
[38] T. Iwasa, J. Phys. Chem. Lett. **15**, 4775 (2024).
[39] J. D. Jackson, *Classical Electrodynamics*, 3rd ed. (Wiley, New York, NY, 1998).
[40] L. Meng, Z. Yang, J. Chen, and M. Sun, Sci. Rep. **5**, 9240 (2015).
[41] K. Fiederling, M. Abasifard, M. Richter, V. Deckert, S. Kupfer, and S. Gräfe, ACS Nano **17**, 13137 (2023).
[42] R. B. Jaculbia, H. Imada, K. Miwa, T. Iwasa, M. Takenaka, B. Yang, E. Kazuma, N. Hayazawa, T. Taketsugu, and Y. Kim, Nat. Nanotechnol. **15**, 105 (2020).
[43] TURBOMOLE V7.7 2022, a development of university of Karlsruhe and Forschungszentrum Karlsruhe GmbH, 1989-2007, TURBOMOLE GmbH, since 2007 available from https://www.turbomole.org.
[44] R. Ahlrichs, M. Bär, M. Häser, H. Horn, and C. Kölmel, Chem. Phys. Lett. **162**, 165 (1989).
[45] S. G. Balasubramani, G. P. Chen, S. Coriani, M. Diedenhofen, M. S. Frank, Y. J. Franzke, F. Furche, R. Grotjahn, M. E. Harding, C. Hättig, A. Hellweg, B. Helmich-Paris, C. Holzer, U. Huniar, M. Kaupp, A. Marefat Khah, S. Karbalaei Khani, T. Müller, F. Mack, B. D. Nguyen, S. M. Parker, E. Perlt, D. Rappoport, K. Reiter, S. Roy, M. Rückert, G. Schmitz, M. Sierka, E. Tapavicza, D. P. Tew, C. van Wüllen, V. K. Voora, F. Weigend, A. Wodyński, and J. M. Yu, J. Chem. Phys. **152**, 184107 (2020).
[46] J. P. Perdew, K. Burke, and M. Ernzerhof, Phys. Rev. Lett. **77**, 3865 (1996).
[47] J. P. Perdew, K. Burke, and M. Ernzerhof, Phys. Rev. Lett. **78**, 1396 (1997).
[48] R. A. Kendall, T. H. Dunning, and R. J. Harrison, J. Chem. Phys. **96**, 6796 (1992).
[49] D. E. Woon and T. H. Dunning, J. Chem. Phys. **98**, 1358 (1993).
[50] M. Noda, S. A. Sato, Y. Hirokawa, M. Uemoto, T. Takeuchi, S. Yamada, A. Yamada, Y. Shinohara, M. Yamaguchi, K. Iida, I. Floss, T. Otobe, K.-M. Lee, K. Ishimura, T. Boku, G. F. Bertsch, K. Nobusada, and K. Yabana, Comput. Phys. Commun. **235**, 356 (2019).
[51] N. Troullier and J. L. Martins, Phys. Rev. B **43**, 1993 (1991).
[52] M. Fuchs and M. Scheffler, Comput. Phys. Commun. **119**, 67 (1999).
[53] K. Yabana and G. F. Bertsch, Phys. Rev. B **54**, 4484 (1996).
[54] H. Nakai, H. Morita, and H. Nakatsuji, J. Phys. Chem. **100**, 15753 (1996).
[55] T. Baba, Y. Imamura, M. Okamoto, and H. Nakai, Chem. Lett. **37**, 322 (2008).
[56] C. A. Ullrich, *Time-Dependent Density-Functional Theory* (Oxford University Press, 2011).
[57] M. Takenaka, T. Taketsugu, and T. Iwasa, J. Chem. Phys. **154**, 024104 (2021).
[58] J. P. Gordon and A. Ashkin, Phys. Rev. A **21**, 1606 (1980).
[59] T. Iida and H. Ishihara, Opt. Lett. **27**, 754 (2002).
[60] T. Iida and H. Ishihara, Phys. Rev. Lett. **90**, 057403 (2003).
[61] T. Kudo and H. Ishihara, Phys. Rev. Lett. **109**, 087402 (2012).
[62] R. P. Feynman, R. B. Leighton, and M. Sands, *The Feynman Lectures on Physics, Vol. I: Mainly Mechanics, Radiation, and Heat* (Addison-Wesley, 1965).
[63] L. D. Landau and E. Lifshitz, *Mechanics*, 3rd ed. (Butterworth-Heinemann, 1976).
[64] K. Nobusada and K. Yabana, Phys. Rev. A **70**, 043411 (2004).
[65] K. Codling and L. J. Frasinski, Contemp. Phys. **35**, 243 (1994).
[66] M. H. S. Peled, F. Morozko, A. Novitsky, P. Maioli, and A. Karabchevsky, Opt Laser. Technol. **168**, 109937 (2024).
[67] X. Li, J. C. Tully, H. B. Schlegel, and M. J. Frisch, J. Chem. Phys. **123**, 084106 (2005).
[68] X. Andrade, A. Castro, D. Zueco, J. L. Alonso, P. Echenique, F. Falceto, and Á. Rubio, J. Chem. Theory Comput. **5**, 728 (2009).
[69] F. P. Bonafé, B. Aradi, B. Hourahine, C. R. Medrano, F. J. Hernández, T. Frauenheim, and C. G. Sánchez, J. Chem. Theory Comput. **16**, 4454 (2020).
[70] H. Uratani and H. Nakai, J. Chem. Theory Comput. **17**, 7384 (2021).

[71] T. Iwasa and K. Nobusada, Phys. Rev. A **80**, 043409 (2009).
[72] M. Takenaka, T. Taketsugu, and T. Iwasa, J. Chem. Phys. **152**, 164103 (2020).
[73] J. w. Kim, H. k. Jeong, K. M. Southard, Y. w. Jun, and J. Cheon, Acc. Chem. Res. **51**, 839 (2018).
[74] S. Duan, Z. Rinkevicius, G. Tian, and Y. Luo, J. Am. Chem. Soc. **141**, 13795 (2019).
[75] H. Inaba, M. Yamada, M. R. Rashid, A. M. R. Kabir, A. Kakugo, K. Sada, and K. Matsuura, Nano Lett. **20**, 5251 (2020).
[76] H. Sugimoto, H. Hasebe, T. Furuyama, and M. Fujii, Small **17**, 2104458 (2021).
[77] H. Sugimoto and M. Fujii, ACS Photonics **8**, 1794 (2021).
[78] J.-Y. Yan, W. Zhang, S. Duan, X.-G. Zhao, and A. O. Govorov, Phys. Rev. B **77**, 165301 (2008).
[79] P. Liu, D. V. Chulhai, and L. Jensen, ACS Nano **11**, 5094 (2017).
[80] A. Mandal, M. A. Taylor, B. M. Weight, E. R. Koessler, X. Li, and P. Huo, Chem. Rev. **123**, 9786 (2023).
[81] K. Yabana, T. Sugiyama, Y. Shinohara, T. Otobe, and G. F. Bertsch, Phys. Rev. B **85**, 045134 (2012).
[82] R. Jestädt, M. Ruggenthaler, M. J. T. Oliveira, A. Rubio, and H. Appel, Adv. Phys. **68**, 225 (2019).
[83] M. Ruggenthaler, J. Flick, C. Pellegrini, H. Appel, I. V. Tokatly, and A. Rubio, Phys. Rev. A **90**, 012508 (2014).
[84] Y.-T. Chuang and L.-Y. Hsu, Phys. Rev. A **109**, 013717 (2024).
[85] H.-S. Tsai, C.-E. Shen, and L.-Y. Hsu, J. Chem. Phys. **160**, 144112 (2024).